J Solid State Electrochem (2012) 16:1723–1732
DOI 10.1007/s10008-011-1582-6

ORIGINAL PAPER

Unusual surface mass changes in the course of the oxygen reduction reaction on platinum and their explanation by using a kinetic model

A. Kriston · B. B. Berkes · P. L. Simon · G. Inzelt · K. Dobos · A. Nemes

Received: 8 August 2011 / Revised: 17 October 2011 / Accepted: 21 October 2011 / Published online: 19 November 2011

Abstract An unusual change of the surface mass with time has been observed during the oxygen reduction reaction on Pt using chronopotentiometry and simultaneous electrochemical quartz crystal nanobalance measurements. A simplified kinetic model of Damjanovic and Brusic, which involves two electrochemical and a chemical step, was analyzed using phase plane analysis. The theoretical analysis predicted that bistability might occur in this system at a certain set of parameter values. The mathematical simulation of the different trajectories explained well the strong influence of the starting potential and the current density on the change of the surface mass observed. Evidence was found that the surface coverage can increase at lower potentials, which can lead to the formation of hydrogen peroxide even if it is energetically unfavorable.

Keywords ORR · Platinum · EQCN · Simulation · Bifurcation

Introduction

The understanding of oxygen reduction reaction (ORR) on platinum surface is crucial concerning the development of efficient and reliable fuel cells. A deeper knowledge of the mechanism could help improve the performance of fuel cells and to decrease the amount of the catalyst used. Many efforts have been done to establish the reaction scheme; however, no final agreement has been reached, yet [1–30]. Most of these studies have dealt with the determination of the apparent Tafel slope at different conditions such as different pH, temperature, and oxygen concentration [2, 3] and with the analysis of the Koutecký–Levich plot [4] by determining the number of electrons involved in the ORR. The coverage–potential relationships using chronoamperometric techniques were also reported [5, 6]. They found that the amount of the oxide, i.e., the coverage, was the same in oxygen-containing and oxygen-free media in the presence of water and that it decreased linearly with the potential (usual behavior). The rate-determining step (RDS) of the ORR was found to be the first electron transfer both at high and at low current densities. The variation of the Tafel slope was thought to be in relation to the surface coverage, which suggested that the rate of the ORR was strongly influenced by the adsorbed intermediates. The deducted reaction scheme was applied successfully for the modeling of fuel cells as well [7, 8].

Considerable advances have been achieved regarding the theory and practical issues of ORR in the last decade. New catalysts were found based on quantum chemical techniques which were used to predict the catalytic behavior of different surfaces. Sidik and Anderson [9] and Nørskov et al. [10] deduced a relationship between ORR activity and oxygen binding energy, which showed a volcano-type plot, by using density functional theory (DFT). The best ORR catalysts among Pt skin catalysts were found near the maximum of the plot, suggesting that the catalytic activity is in connection with the adsorption bond strength of the different intermediates. Pt electrode immersed in oxygen-

A. Kriston (✉) · B. B. Berkes · G. Inzelt · K. Dobos · A. Nemes
Department of Physical Chemistry, Institute of Chemistry,
Eötvös Loránd University,
Pázmány Péter sétány 1/A,
Budapest 1117, Hungary
e-mail: info@fuelcell.hu

P. L. Simon
Department of Applied Analysis and Computational Mathematics,
Institute of Mathematics, Eötvös Loránd University,
Pázmány Péter sétány 1/C,
Budapest 1117, Hungary

free media has been extensively studied by a variety of techniques such as X-ray photoelectron spectroscopy [11], atomic force microscopy [12], electrochemical quartz crystal nanobalance (EQCN) [13], etc. Much less combined electrochemical/non-electrochemical investigations have been carried out in oxygen-saturated solution.

In this paper, the results on the ORR at platinum electrodes in oxygen-saturated aqueous acidic solutions that were obtained using different electrochemical techniques (chronopotentiometry and cyclic voltammetry) in combination with EQCN measurements as well as mathematical simulation will be presented. Based on a relatively simple scheme of the reaction mechanism introduced by Damjanovic and Brusic [2], the time dependences of the potential and surface mass responses were calculated and compared with the experimental results. It was hoped that the mathematical analysis and simulation would provide an explanation of the unusual variation of the surface mass changes observed.

The dynamic behavior of this system was investigated analytically in [14] using the methods of phase plane analysis, such as Poincaré–Bendixson theory, Bendixson's criterion, and the index of critical points [15]. These calculations have revealed that bistability may occur in this system at high values of the kinetic parameters. This means that two different values of the current and surface coverage belong to a fixed value of the potential. It was also proven mathematically that there were no periodic solutions of the kinetic system; hence, the current tends to its stationary value for long times at every parameter.

Model description

A widely accepted mechanism of ORR at platinum electrodes in acidic media was introduced by Damjanovic and Brusic [2] and used by many authors, recently, e.g., Xu et al. [7] as well as Franco and Tembely [8]. Quantum mechanical simulations [16] have also reached similar conclusions; however, inherent approximations within those models may not be describing the true complexity of the ORR under electrochemical environments. Therefore, we consider the reaction as follows. The first step is a very fast oxygen adsorption, and then an electrochemical reaction takes place in which an adsorbed O_2H molecule is formed according to Eq. 1 through the hydrogenation of the oxygen. The next step is a chemical reaction; however, the exact pathway has not been revealed. The simplest reaction between the adsorbed O_2H and a water molecule results in adsorbed OH species [8], as shown in Eq. 2. If the dissociation of O_2H happens, there are two possible paths. First, O reacts with a proton in an electrochemical step forming OH, or O reacts with water forming two OH, which was found by Ogasawara et al. [17]. The Pt surface is always covered by water molecules [18]; therefore, it is reasonable to simplify the chemical steps to 2. The difference between the two pathways is the number of the formed OH, i.e., three adsorbed OH forms in the simplified model and two OH forms in the more complicated model. Finally, the adsorbed OH species are reduced to water in a fast electrochemical step presented in Eq. 3.

$$O_2 + H^+ + e^- \rightarrow O_2H(\text{ads}), \quad k_1', \quad k_{-1}' \tag{1}$$

$$O_2H(\text{ads}) + H_2O \rightarrow 3OH(\text{ads}), \quad k_2', \quad k_{-2}' \tag{2}$$

$$OH(\text{ads}) + H^+ + e^- \leftrightarrow H_2O, \quad k_3', \quad k_{-3}' \tag{3}$$

where $k_1'(i \in \{-3,-2,-1,1,2,3\})$ is the rate constant of the reactions.

It should be mentioned that several more complicated mechanisms have been assumed [1]. However, those are in fact the extended version of the one considered herein. In the case when more reactions are considered, the number of unknown parameters (rate coefficients, standard potentials) that should be taken into account increases, which certainly increases the uncertainty. Therefore, we have neglected several possible reactions that might be involved in the overall reaction mechanism and used the original scheme of Damjanovic and Brusic. For instance, the formation of H_2O_2 was neglected. This choice might be justified because H_2O_2 formation occurs on the Pt electrode at high overpotentials only, and according to the DFT calculations, this process is energetically unfavorable [19]. However, the results of the DFT calculations cannot be used without certain reservations since in those calculations simplified models and several assumptions have been made. H_2O_2 may also be formed at defect sites, which are not yet modeled by DFT. With this simplification, it does not mean that the authors would reject the formation of H_2O_2 entirely since even in the scheme considered herein H_2O_2 formation may occur upon the release of O_2H radicals. In the case of aqueous sulfuric acid electrolytes, the activities of water and hydrogen ions are constant and can be integrated into the rate constants. For the adsorption process, Langmuir conditions are assumed. This requirement is fulfilled if the coverage is lower than 0.2, i.e., the current density is high enough [5]. According to the mechanism described in Eqs. 1–3, the reaction rates can be expressed as follows:

$$v_1 = k_1\theta_s \exp\left(-\frac{\beta_1\left(E-E^{0,1}\right)F}{RT}\right) - k_{-1}\theta_{O_2H} \quad \exp\left(\frac{(1-\beta_1)\left(E-E^{0,1}\right)F}{RT}\right) \tag{4}$$

$$v_2 = k_2\theta_{O_2H}\theta_s^2 - k_{-2}\theta_{OH}^3 \quad (5)$$

$$v_3 = k_3\theta_{OH}\exp\left(-\frac{\beta_2\left(E-E^{0,3}\right)F}{RT}\right) - k_{-3}\theta_s \quad \exp\left(\frac{(1-\beta_2)\left(E-E^{0,3}\right)F}{RT}\right) \quad (6)$$

where,

$$k_1 = k_1^{'}c_{O_2}c_{H^+}, \quad k_{-1} = k_{-1}^{'}, \quad k_2 = k_2^{'}, \quad k_{-2} = k_{-2}^{'},$$
$$k_3 = k_3^{'}c_{H^+}, \quad k_{-3} = k_{-3}^{'}c_{H_2O}$$

θ_s	is the ratio of free surface spaces per unit surface area
c_{O2}	is the oxygen concentration in the liquid phase
c_{H^+}	is the hydrogen ion concentration
c_{H_2O}	is the water concentration in the liquid phase
β_j	is the transfer coefficient, $j \in \{1,2\}$
E	is the electrode potential vs. SCE
$E^{0,k} = -\frac{\Delta G^{0,k}+\Delta H^k}{F}$	are the respective standard potentials, $k \in \{1,3\}$
$\Delta G^{0,k}$	is the activation energy of the kth reaction at low coverage
ΔH^k	is the heat of adsorption of the reactant and product in the kth reaction (it is assumed that ΔH^k does not change with coverage, i.e., Langmuirian conditions prevail)
F	is the Faraday constant
R	is the gas constant
T	is the temperature
θ_{O_2H}	is the coverage of the O_2H molecule
θ_{OH}	is the coverage of the OH molecule

The kinetic equations take the form

$$\dot{\theta}_{OH} = 3v_2 - v_3 \quad (7)$$

$$\dot{\theta}_{O_2H} = v_1 - v_2 \quad (8)$$

where the dot denotes differentiation with respect to time. For a given value of the potential, this is a nonlinear system of ordinary differential equations. The solutions of this system cannot be expressed explicitly; hence, phase plane analysis and numerical methods have to be applied. Solving the system numerically, the voltage can be obtained for the chronopotentiometric case from the following differential equation

$$\frac{dE}{dt} = \frac{(I+F(v_1+v_3))}{C} \quad (9)$$

where C is the double-layer capacitance. It was assumed that only one species bonded to an active site at total coverage, which was 210 μC cm^{-2} (2.17×10^{-9} mol cm^{-2}) for a flat Pt surface. The surface mass has been calculated by the following assumption:

$$m_{surf} = N_{total}(\theta_{OH}M_{OH} + \theta_{O_2H}M_{O_2H})\cdot f_R \quad (10)$$

where M_x is the molar mass of the species, N_{total} is the free site per unit area, and f_R is the roughness factor of the surface, currently assumed to be 5.

The following nonlinear ordinary differential equations were used in the simulations:

$$\dot{\theta}_1 = 3K_2\theta_2\theta_s^2 - 3L_2\theta_1^3 - K_3\theta_1 + L_3\theta_s \quad (11)$$

$$\dot{\theta}_2 = K_1\theta_s - L_1\theta_2 - K_2\theta_2\theta_s^2 + L_2\theta_1^3 \quad (12)$$

where

$$\theta_1 = \theta_{OH}, \quad \theta_2 = \theta_{O_2H}, \quad \theta_s = 1 - \theta_1 - \theta_2$$

and

$$K_1 = k_1\exp\left(-\frac{\beta_1(E-E_1)F}{RT}\right), \quad K_2 = k_2, \quad K_3 = k_3\exp\left(-\frac{\beta_2(E-E_2)F}{RT}\right)$$
$$L_1 = k_{-1}\exp\left(\frac{(1-\beta_1)(E-E_1)F}{RT}\right), \quad L_2 = k_{-2}, \quad L_3 = k_{-3}\exp\left(\frac{(1-\beta_2)(E-E_2)F}{RT}\right)$$

The standard potentials, E_1 and E_2, used herein differ from the ordinary values tabulated for these reactions due to the energy of adsorption of the species on the surface. The adsorption bond strengths from the DFT data were used to estimate standard potentials. The standard potentials for the surface reaction Eqs. 1 and 3 were calculated by the following relationships:

$$E^{0,1} = E^{bulk,1} + U_{surface}^{O_2H} - U_{surface}^{O_2} \quad (13)$$

$$E^{0,3} = E^{bulk,3} + U_{surface}^{H_2O} - U_{surface}^{OH} \quad (14)$$

There is no DFT calculation for the polycrystalline Pt surface available; however, according to Zinola et al. [20] Pt (111) should behave similarly to poly-Pt since Pt(111) has the most packed structure and therefore has more active sites than, e.g., Pt(100). In the following, the average of the binding energies of the different sites (e.g., ring, flat, etc.) on Pt(111) calculated by DFT methods (see Table 1) has been used for the calculation of the surface standard potentials (Table 2). It must be mentioned that the calculated binding energies span in a very broad range, in the case of oxygen between 0.1and 1.95 eV [21]. The binding energies calculated by Keith et al. [21] were the closest to the electrochemical environment; hence, it was used for our calculations. The measured binding energy of oxygen on Pt is in the range of 0.3–0.5 eV [22], which is approximately the average of the energies of the

Table 1 Binding energies of the different intermediates of the ORR on Pt(111)

Species/bonding sites	Binding energies (eV)	
	Keith et al. [21]	Average
OOH		1.285
Ring	1.39	
Non-ring	1.18	
OH	2.42	2.42
O_2		0.58
Bridge	0.62	
fcc	0.96	
Tilted	0.17	
H_2O	0.5	0.5

different binding sites that have been obtained by different calculations. The data determined in electrochemical environment are not available; therefore, the calculated binding energies were used for the simulations.

The kinetic coefficients were estimated from our measurements and the observations of others [3]. The slowest process, i.e., RDS, was thought to be the hydrogenation of oxygen (Eq. 1), while the highly irreversible chemical step (Eq. 2) was assumed to be the fastest [2]. The parameters in Table 3 were used in the simulations.

Experimental

Reagents

All the reagents used were of analytical grade. Sulfuric acid (Merck) was used as received. The solutions were prepared with double distilled water (Millipore). The oxygen was generated in situ using a second Pt electrode immersed in the same solution. The potentials were controlled by a bipotentiostat. The potential of the oxygen generation was 1.9 V vs. sodium-saturated calomel electrode (SCE).

Electrochemical instrumentation

A four-electrode electrochemical cell was used (Fig. 1). The working electrode for the investigation of ORR was an EQCN platinum electrode. A second platinum working electrode was applied for the in situ oxygen generation for the sake of purity. A platinum wire counter electrode was separated from the cell, with two porous glass frits.

Five-megahertz AT-cut crystals of 1-in. diameter (Stanford Research Systems, SRS, USA) were used in the EQCN measurements. Each side of the crystals was coated with a titanium underlayer and platinum. Only one side of the crystals with a projected surface area of $A=1.37$ cm^2 was exposed to the electrolyte solution. The piezoelectrically active area was equal to 0.33 cm^2. The crystals were mounted in the holder made from Kynar and connected to an SRS QCM100 unit (quartz crystal microbalance controller). The polished crystals were optically clear; according to the SRS certification, their average surface roughness was approx. 5 nm, which was proven by Berkes et al. [23]. The change of the frequency was followed with a Fluke PM6685 universal frequency counter. A Biologic VSP multipotentiostat was used for the measurements and for the oxygen evolution.

Numerical simulation

Because of the exponential terms in the reaction rates, the kinetic differential equations are stiff equations. We used the stiff ODE solver of MATLAB to get the numerical solutions of these stiff differential equations and to determine the trajectories in the phase plane. The bifurcation curves were constructed using the parametric representation method [24].

Results and discussion

The reaction phase planes

A detailed mathematical analysis of the system (Eqs. 1–6) was made by Csörgő and Simon [14] using the Poincaré–Bendixson theory and the parametric representation method. They concluded some general analytical results: the system (Eqs. 1–6) has no periodic orbit and bistability may occur at certain electrode potentials. The general behavior of the system was the following when the standard potentials listed in Table 2 were applied (i.e., $E^{0,1} \leq E^{0,3}$) and the other kinetic parameters were arbitrary. When E was close enough to 1 V vs. SCE (e.g., at open circuit voltage, OCV), there was a single stationary point. For

Table 2 Calculated standard potentials

Reaction step	E_{bulk} (V)				Standard potential (V)
	Sidik et al. [16]	Wroblowa et al. [5]	Inzelt	Average	
$1./E^{0,1}$		−0.13	−0.046	−0.088	0.61
$3./E^{0,3}$	2.81		2.38	2.595	0.89

Table 3 Kinetic parameters at 298 K used in the calculation

Rate coefficients	Unit	Value
$k_1 = k_{-1}$	$cm^{-2}\ s^{-1}$	10^{-4}
k_2	$cm^{-2}\ s^{-1}$	0.8×10^{-2}
k_{-2}	$cm^{-2}\ s^{-1}$	10^{-4}
$k_3 = k_{-3}$	$cm^{-2}\ s^{-1}$	10^{-3}
A	cm^2	1.37

smaller values of E, bistability occurred. At these values of E, three stationary points existed: one of them was a saddle point and the other two points were stable. Decreasing the value of E further, a single stationary point appeared again. This is shown in Fig. 2 where the coverage ($\theta_{OH} + \theta_{O_2H}$) is plotted against E for fixed values of the kinetic parameters (Table 3). It can be seen that there are three steady states when E is between approximately 0.24 and 0.35 V, and there is a unique stationary point when E is outside this interval. The dotted line shows the saddle point for the third stationary (but not stable) solution.

Two typical phase portraits calculated are displayed in Fig. 3 at different electrode potentials. Figure 3a, b shows the potential outside the region of the bistability and a case when bistability occurred, respectively. The arrows show the evolution of the coverage in time. For example, if the initial coverage started from point B (Fig. 3a), it continuously decreased until the stationary point (circle) following the dotted trajectory.

As seen in Fig. 3b, the system had two stable points (attractor, circle) and one saddle point (which separates the two stable points, cross). The stable manifold of the saddle

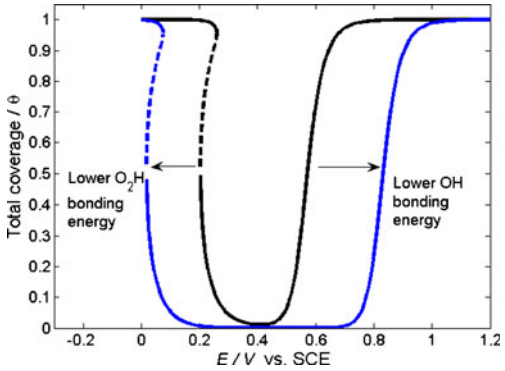

Fig. 2 Dependence of the total coverage, θ, on the potential, E, vs SCE. For small (close to zero) and large (close to 1) values of E, there is a unique stationary state; for the E (*dotted line*) values in between, bistability occurs (saddle point). *Arrows* show the effect of the lower binding energy (approx. 0.2 eV) of the adsorbed oxygen species

point (formed by the two trajectories that converge to the saddle) divided the phase plane into two parts that were the basins of attraction for the stable points. Examining the possible trajectories, a very interesting behavior can be seen. If the initial surface coverage started from point C (Fig. 3b), the coverage decreased until point D (usual behavior), at which point it turned back and increased (unusual behavior) again while it reached the stable point (circle). It clearly showed that the surface coverage was not a linear function of the potential. It is also interesting that, in both cases, there existed an attracting manifold to which the other trajectories converged first.

Consequently, the starting electrode potential at a given set of potential-dependent rate coefficients and the initial state of the electrode strongly influences the time-dependent

Fig. 1 Electrochemical cell

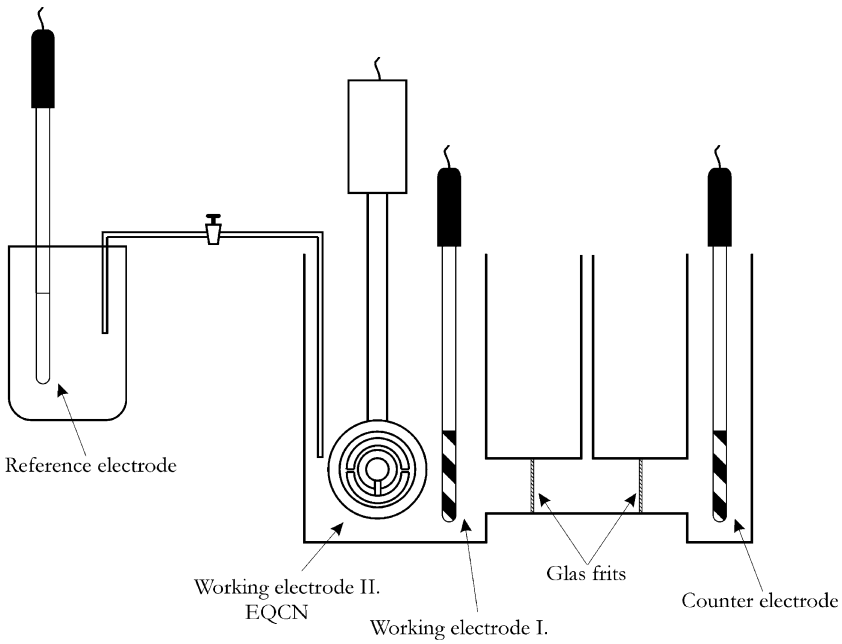

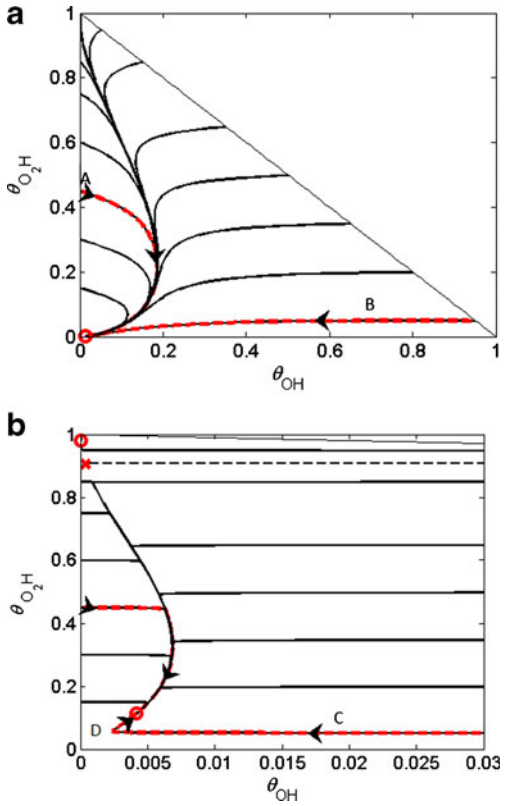

Fig. 3 The $(\theta_{OH}, \theta_{O_2H})$ phase planes of the system (Eqs. 1–6) at E=0.53 V (**a**) and at E=0.33 V (**b**) vs. SCE. The *circles* denote the stable stationary points and the *cross* denotes the saddle point. *Arrows* show the time dependence of the trajectories

behavior of the system. The electrode potential determines whether a bistability, i.e., the bifurcation behavior during the ORR, occurs or not. The kinetic parameters of the chemical reaction (k_2,k_{-2}) influence the position of the system within the domain of one or three stable steady states. The surface energetics has the highest importance on the coverage (Fig. 2). If the binding energy of O_2H is smaller, then the hydrogenation of the oxygen molecules (Eq. 1) can take place at a lower energy (therefore the more negative the $E^{0,1}$), the formation of O_2H is shifted to lower electrode potentials and the window of the near zero surface coverage broadens, which can delay the formation of H_2O_2. The effect of $E^{0,3}$ (formation of water) is similar. The lower is the binding energy of OH, the more positive is the $E^{0,3}$, which leads to the broadening of the region of the zero surface coverage. The same effect was observed by Stamenkovic et al. [25] when a Pt_3Ni catalyst was used, whose activity was much higher than Pt(111). The increased activity was supposed to be caused by the smaller binding energy of O_{ads}, which resulted in smaller OH coverage at small overpotentials and shifted the peroxide formation to more negative potentials.

At low potentials, the surface is covered with O_2H radicals, eventually fully. This accumulation may be followed by the formation of hydrogen peroxide, which was observed by many authors [25, 26], even if it is energetically unfavorable, in accordance with the DFT calculations. If the zero coverage region is too wide, i.e., the formation of O_2H radicals would overlap with the hydrogen underpotential deposition region, the coverage with respect to O_2H species might be much lower or nonexistent due to the following reaction:

$$O_2H(ads) + H(ads) \rightarrow H_2O_2 \qquad (15)$$

Time-dependent functions

The analysis of the global bifurcation diagram indicated that the potential vs. time and surface mass vs. time plots

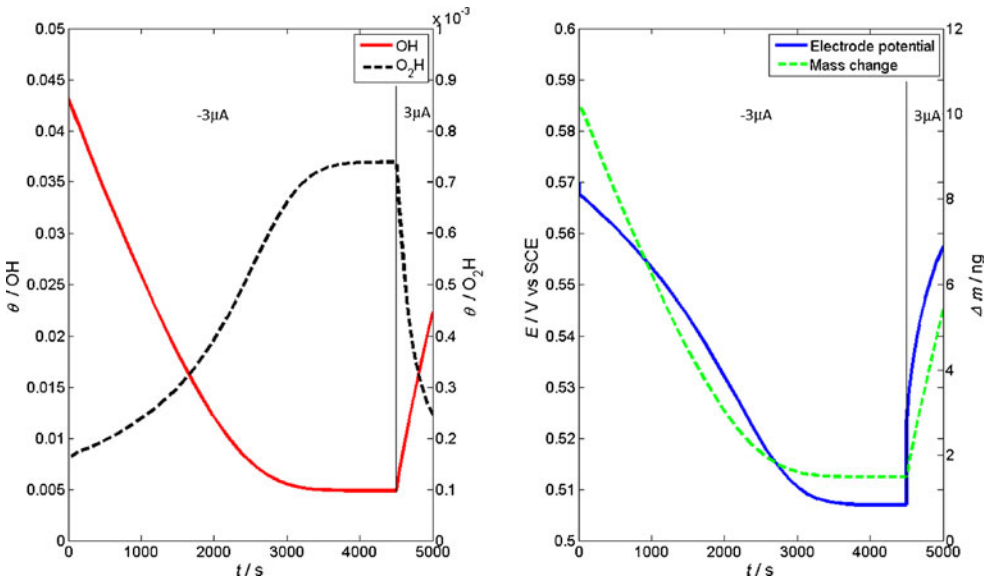

Fig. 4 Simulated chronopotentiometric diagrams starting from steady-state coverage at 0.57 V vs. SCE. The applied current was I=−3 μA during the first 4,500 s and I=3 μA in the last 500 s

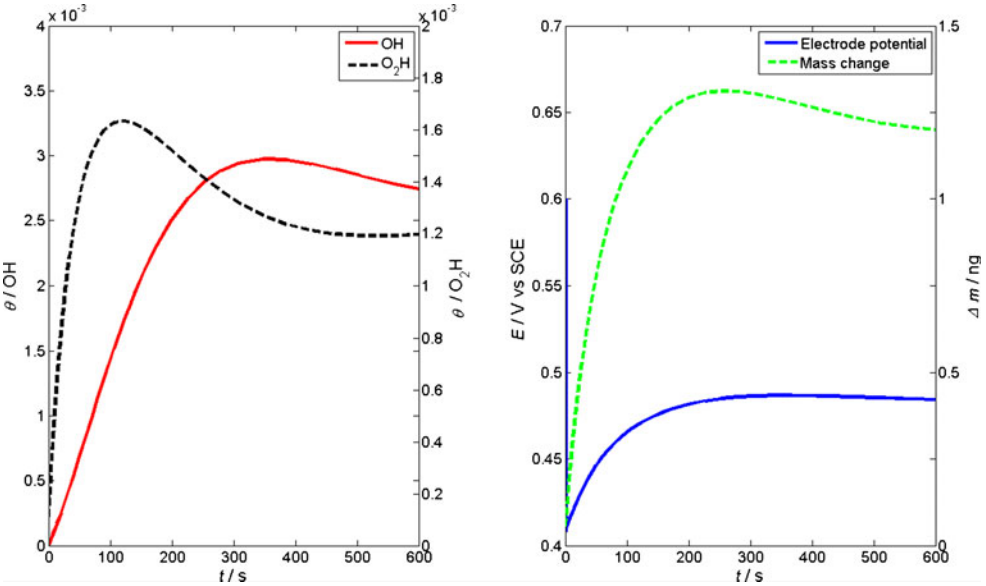

Fig. 5 Simulated chronopotentiometric diagrams starting from $\theta_{OH}=5\times10^{-6}$ and $\theta_{O2H}=1\times10^{-4}$ coverage at 0.6 V vs. SCE. Applied current was $I=-5$ μA

can be very different regarding the initial coverage and the potential or current applied. Figure 4 shows the expected variation of potential, coverage, and surface mass vs. time during the reduction (0–4,500 s) and oxidation (4,500–5,000 s). In the reduction step, the mass and the potential decreased until the steady state was reached. Regarding the phase plane analysis in this potential range, there is only a single solution: the OH coverage becomes zero but that of O_2H slightly increases (Fig. 3a, trajectory B). It is also shown that an application of an anodic current (at 4,500 s) results in the expected potential and mass increase, respectively. This behavior is said to be the normal behavior of the surface mass and potential.

Figure 5 shows the unusual behavior of the surface mass and potential, i.e., the potential quickly dropped in the first few seconds and then started to increase before it decreased to the stationary value. Simultaneously, the mass increased, then decreased slightly, and eventually reached the steady-state value. This type of overshoot phenomenon can happen when the initial coverage starts from the top left corner in Fig. 3a (e.g., point A), which can be realized in real systems if the initial coverage is different from the steady-state value of the starting potential, i.e., θ_{OH} is much smaller while θ_{O_2H} is higher than the steady-state values.

In light of the results and discussion of the simulation, the unusual mass changes observed in the course of the EQCN measurements shown in Fig. 6 can be explained. The curve displayed has been detected after the following treatment. First, the electrode was kept potentostatically at −0.18 V in the presence of oxygen for 10 min. Then, the circuit was interrupted and the potential and mass changes were followed at OCV for 5 min. Due to the presence of oxygen, the potential increased. Then—not waiting for the establishment of the steady state—a cathodic current ($I=-5$ μA) was applied. Therefore, the initial coverages were different from the steady-state values, i.e., lower OH and higher O_2H coverage existed. Under this condition, as had been predicted by the simulation (Fig. 5), first, the potential dropped but shortly after increased (see Fig. 6), while a simultaneous mass increase was observed. The mass excursion is due to the reaction of the excess O_2H with water molecules in the chemical step (Eq. 2), resulting in adsorbed OH species.

In order to control the surface state, i.e., the initial coverage which plays a decisive role concerning the time dependence of the events after applying a cathodic current the following protocol has been applied for conditioning the electrode surface: (1) the potential was swept from −0.15 to 1.00 V, with 10 mV/s; (2) the solutions were saturated with oxygen for at least 1 h prior to the measurement; and then (3) cathodic currents of different magnitudes were applied.

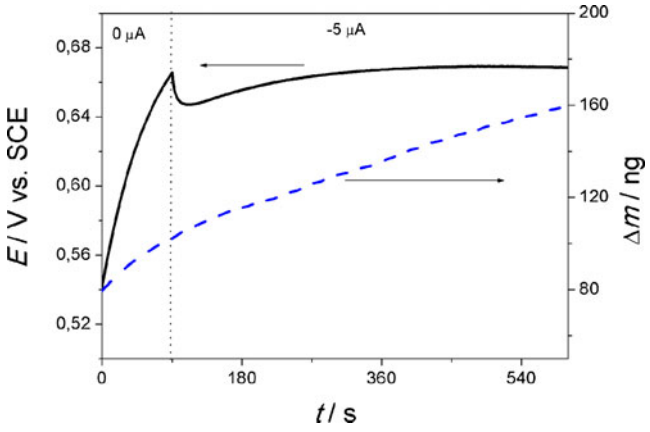

Fig. 6 Measured chronopotentiometric curve in the presence of oxygen. The applied cathodic current was −5 μA after the electrode was kept at −0.18 V vs. SCE and followed at OCV, but interrupted before the establishment of the steady state

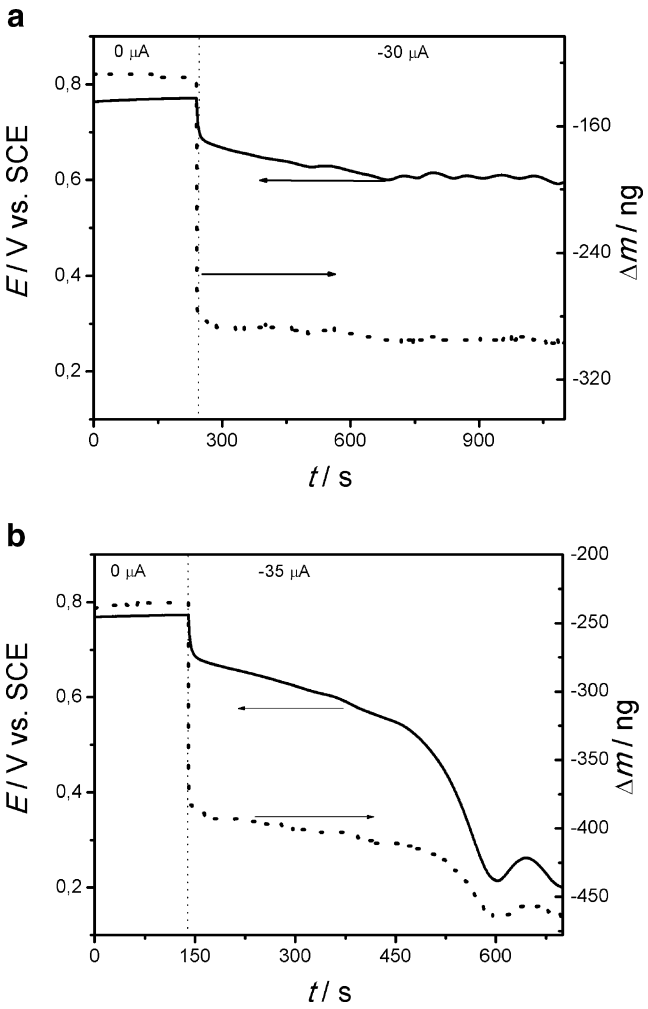

Fig. 7 Measured chronopotentiometric curve at I=−30 μA (**a**), and I=−35 μA (**b**)

The simultaneous changes of potential and surface mass as a function of time in the course of step (3) are displayed in Fig. 7a. This shows that after applying −30 μA cathodic current, both the potential and the surface mass have reached practically stable values. However, as can be seen in Fig. 7b, after the application of only a slightly higher cathodic current (−35 μA), a rather different picture appeared. The most striking phenomenon was that after a long decrease in both the potential and the surface mass, a relatively fast increase of both the potential and mass appeared, which was followed by a further decrease of both quantities. It should be mentioned that in both diagrams, the reduction started from a steady-state potential and surface mass state (opposite to Fig. 6), which can be seen in the first 300 s.

The difference between the two diagrams in Fig. 7 can be explained by the different phase portraits in Fig. 3. The curves in Fig. 7a correspond to trajectory B in Fig. 3a and the time-dependent plots of Fig. 5, where no bistability occurred because the potential stabilized at a relatively high value (0.6 V vs. SCE). In Fig. 7b, however, the potential dropped below the critical value; hence, the special trajectory of the bistability could appear (turning point D in Fig. 3b). If the bistability occurs, there exist such trajectories, when the mass increases, even if the initial coverage starts from the steady-state value. This phenomenon was calculated in Fig. 8, which shows that the coverage of the OH intermediate decreased while the O_2H intermediate increased. Having reached the near zero value, the OH coverage started to increase again following the special turning trajectory. While the initial coverage of the O_2H radical was very low (near zero), therefore its overall contribution to the mass change was minimal. The main factor of the mass excursion was the decreasing–increasing coverage of the OH radical. It should

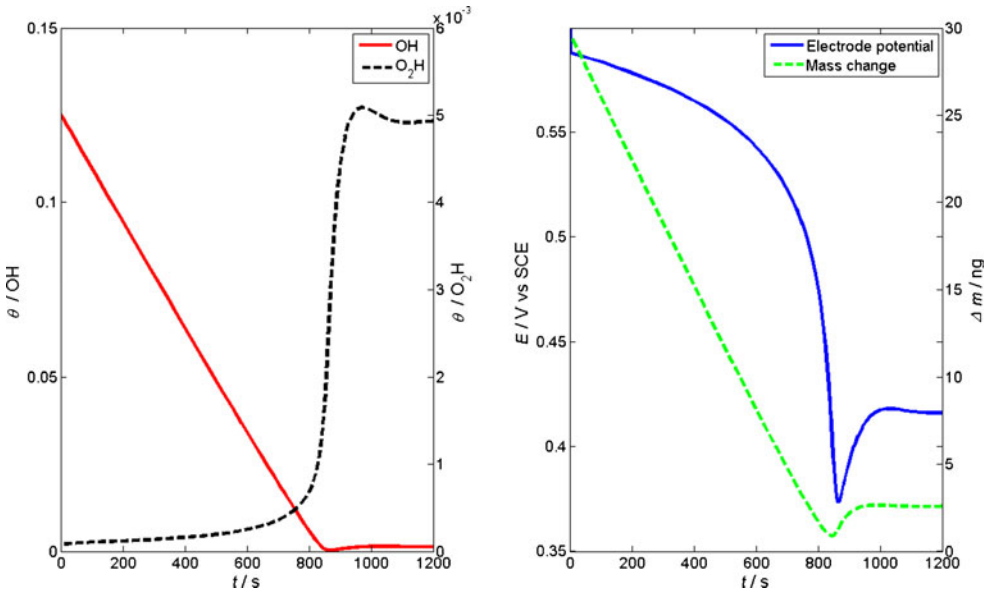

Fig. 8 Simulated chronopotentiometric curves and coverage at −20 μA in the presence of oxygen, starting from the steady-state coverage at 0.6 V vs. SCE

be mentioned that if the current applied becomes much higher than the diffusion-limited current of the oxygen reduction, which depends on the stirring and the oxygen concentration, the potential does not reach a steady value, but decreases further. The simulated curves provide a general explanation of the effects observed; however, two important factors have been neglected in the simulation. First, the concentration of oxygen at the electrode was assumed to be constant, which is hardly valid in real systems near the surface of the EQCN electrode. Second, there is a continuous variation of the double layer due to the potential changes and the adsorption/desorption of other species like SO_4^{2-} [27].

In spite of the side effects, the simulated chronopotentiometric curves (Fig. 8) can fit qualitatively well with the measured ones (Fig. 7). The surface coverage regarding the oxide-containing species is originated from three sources: (1) at high anodic potentials, Pt–O and Pt–OH [28, 29] are formed overwhelmingly from the water discharge, in accordance with the results of the quantum mechanical model used by Bockris and Abdu [30]. Therefore, the presence or the absence of oxygen makes no difference. (2) At lower potentials in the presence of oxygen, Pt–OH species are also formed by the reactions (Eq. 2). (3) The coverage of platinum surface by O_2H species originated from reaction Eq. 1 becomes substantial at low potentials and occurs only when the electrode is in contact with oxygen-containing media. Even in the presence of oxygen, there is a potential interval where the coverage with respect to the oxygen-containing species is low.

Conclusions

It was demonstrated that the change of the surface mass with time during the oxygen reduction reaction on platinum was strongly affected by the starting potential and the current density applied. By using a kinetic model of Damjanovic and Brusic [2, 3], a mathematical simulation was applied, which can provide an explanation of the unusual behavior with respect to the potential and the surface mass change observed. The reaction scheme was analyzed using phase plane analysis, and it turned out that bistability occurs in this system at a certain set of parameter values. The detailed mathematical study and the proof of the results presented in [14] are based on the Poincaré–Bendixson theory and the parametric representation method. Different time-dependent solutions were simulated and compared with the measured data. It can be concluded that the coverage of species OH and O_2H changes as a function of potential and that their ratio depends on the starting potential during the oxygen reduction reaction.

The phase plane analysis showed that the surface was mainly covered with OH at high potentials, which decreased to zero at more negative potentials, meanwhile the O_2H coverage increased. The bifurcation started from approx. 0.4 V vs. SCE, where two stable surface states can be observed. At very negative potentials (<0.2 V vs. SCE), the surface was covered with O_2H in every case. An unusual behavior of the mass change of Pt electrode was found (mass increase during the reduction), and it can be interpreted in terms of the special trajectory of the system which can occur if the initial coverage is different from the respective steady-state coverage or with the existence of bistability. Further improvement of the numerical model is in progress by taking diffusion and peroxide formation into account.

Acknowledgments Financial supports of the National Office of Research and Technology (OMFB-00356/2007 and OM-00121-00123/2008) and National Scientific Research Fund (OTKA K71771) as well GVOP-3.2.1-2004-040099 are acknowledged.

References

1. Bockris JO'M, Khan SUM (1993) Surface electrochemistry: a molecular level approach. Plenum, New York, p 286
2. Damjanovic A, Brusic V (1967) Electrochim Acta 12:615–628
3. Sepa DB, Vojnovic MV, Damjanovic A (1980) Electrochim Acta 26:781–793
4. Schmidt TJ, Gasteiger HA, Stab GD, Urban PM, Kolb DM, Behm RJ (1998) J Electrochem Soc 145:2354–2358
5. Wroblowa H, Rao MLB, Damjanovic A, Bockris JO'M (1967) J Electroanal Chem 15:139–150
6. Xu H, Kunz R, Fenton JM (2007) Electrochem Solid-State Lett 10:B1–B5
7. Xu H, Song Y, Kunz R, Fenton JM (2005) J Electrochem Soc 152:A1828–A1836
8. Franco AA, Tembely M (2007) J Electrochem Soc 152:B712–B723
9. Sidik RA, Anderson AB (2002) J Electroanal Chem 528:69–76
10. Nørskov JK, Rossmeisl J, Logadottir A, Lindqvist L, Kitchin JR, Bligaard T, Jónsson H (2004) J Phys Chem B 108:17886–17892
11. Wakisaka M, Suzuki H, Mitsui S, Uchida H, Watanabe M (2009) Langmuir 25:1897–1900
12. Wakisaka M, Asizawa S, Uchida H, Watanabe M (2010) Phys Chem Chem Phys 12:4184–4190
13. Jerkiewicz G, Vatankhah G, Lessard J, Soriaga MP, Park YS (2004) Electrochim Acta 49:1451–1459
14. Csörgő G, Simon PL (2010) Annales Univ Sci Budapest de R Eötvös Nom Sect Mat 53:45–47
15. Perko L (2001) Differential equations and dynamical systems. Springer, New York
16. Sidik RA, Anderson AB, Subramanian NP, Kumaraguru SP, Popov BN (2006) J Phys Chem B 110:1787–1793
17. Ogasawara H, Näslund LÅ, MacNaughton JB, Anniyev T, Nilsson A (2008) ECS Trans 16(2):1385–1394
18. Wakisaka M, Suzuki H, Mitsui S, Uchida H, Watanabe M (2010) Langmuir 25:1897–1900
19. Tripkovic V, Skúlason E, Siahrostami S, Nørskov JK, Rossmeisl J (2010) Electrochim Acta 55:7975–7981
20. Zinola CF, Luna AMC, Triaca WE, Arvia AJ (1994) J Appl Electrochem 24:119–125
21. Keith JA, Jerkiewicz G, Jacob T (2010) ChemPhysChem 11:2779–2794
22. Gland JL (1980) Surf Sci 93:487–514

23. Berkes BB, Maljusch A, Schuhmann W, Bondarenko AS (2011) J Phys Chem C 115:9122–9130
24. Simon PL, Farkas H, Wittmann M (1999) J Comp Appl Math 108:157–176
25. Stamenkovic VR, Fowler B, Mun BS, Wang GF, Ross PN, Lucas CA, Markovic NM (2007) Science 315:493–497
26. Alonso-Vante N (2010) ChemPhysChem 11:2732–2744
27. Inzelt G, Berkes BB, Kriston A, Székely A (2011) J Solid State Electrochem 15:901–915
28. Birss VI, Chang M, Segal J (1993) J Electroanal Chem 35:181–191
29. Inzelt G, Berkes BB, Kriston A (2010) Electrochim Acta 55:4742–4749
30. Bockris JO'M, Abdu R (1998) J Electroanal Chem 448:189–204